Accepted Manuscript

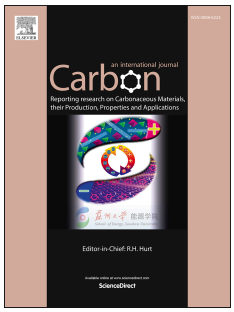

Modulated enhancement in ion transport through carbon nanotubes by lipid decoration

Jiaojiao Liu, Bing Yuan, Xuewu Wu, Jingliang Li, Fangming Han, Yujiang Dou, Muzi Chen, Zhaohui Yang, Kai Yang, Yuqiang Ma

PII: S0008-6223(16)30889-2

DOI: 10.1016/j.carbon.2016.10.030

Reference: CARBON 11389

To appear in: *Carbon*

Received Date: 3 August 2016

Revised Date: 11 October 2016

Accepted Date: 13 October 2016

Please cite this article as: J. Liu, B. Yuan, X. Wu, J. Li, F. Han, Y. Dou, M. Chen, Z. Yang, K. Yang, Y. Ma, Modulated enhancement in ion transport through carbon nanotubes by lipid decoration, *Carbon* (2016), doi: 10.1016/j.carbon.2016.10.030.

Modulated enhancement in ion transport through carbon nanotubes by lipid decoration

Jiaojiao Liu[a,b], Bing Yuan[a,b,*], Xuewu Wu[a,b], Jingliang Li[e], Fangming Han[f], Yujiang Dou[c], Muzi Chen[d], Zhaohui Yang[a,b,*], Kai Yang[a,b,*], and Yuqiang Ma[a,b,g]

[a] Center for Soft Condensed Matter Physics and Interdisciplinary Research, [b] College of Physics, Optoelectronics and Energy, [c] School of Electronic and Information Engineering, [d] Analysis and Test Center, Soochow University, Suzhou, 215006, P. R. China.

[e] Institute for Frontier Materials, Deakin University, Waurn Ponds, Vic, 3216, Australia.

[f] Institute of Solid State Physics, Chinese Academy of Sciences, Hefei, 230031, P. R. China

[g] National Laboratory of Solid State Microstructures and Department of Physics, Nanjing University, Nanjing, 210093, P. R. China.

ABSTRACT. Biomimetic channels based on carbon nanotubes (CNTs) with fast and selective transport have attractive applications in many fields. In this work, a remarkable and modulated enhancement in the ion transport rate through CNTs is facilitated by means of lipid decoration,

* Corresponding authors.

Tel/Fax: 86 512 65220239. E-mail: yuanbing@suda.edu.cn (B.Y.). Tel/Fax: 86 512 69156391. E-mail: yangzhaohui@suda.edu.cn (Z.Y.). Tel/Fax: 86 512 65220239. E-mail: yangkai@suda.edu.cn (K.Y.).

by a factor of up to 20 times. A type of CNT membrane is firstly prepared, composed of well aligned multi-wall carbon nanotubes with an inner size of ~10 nm. An inter-diffusion method is used to efficiently incorporate lipids within the CNTs. It is found that the lipid phase state as well as the surface property of the tubes' inner walls corporately determine the assembly behavior, such as location and stability of lipids, which further influence the ion transport rate through the tubes. For example, the incorporation and self-assembly of liquid-phase DOPC and polymerized Diyne-PC within the tubes induces an enhancement in steady ion transport rate through CNTs by a factor of 5 and 20 times, respectively. In contrast, the gel-phase DPPC prefers to stay at tube tips, which increases the ion transport rate during the initial stage only. This work provides a practical guide to regulate the ion transport behaviors through CNTs for versatile applications.

1. Introduction

Owing to their unique and outstanding properties, extensive research has been carried out on carbon nanotubes (CNTs) for practical applications in such as novel nanomaterial science and biomedical fields [1−4]. In particular, CNTs offer the potential as a candidate of mimicking biological channels due to their inner-core diameter in the size range of many proteins and other important biological macromolecules [5,6]. However, compared with biological protein channels, which can realize extraordinarily complicated cellular functions such as selective transport and high-efficient transmission of various chemicals across cell walls, the fabrication of such CNT-based biomimetic channels still poses a significant challenge [7–9].

In fact, transport phenomena through the hollow conduits of CNTs have been attracting intense interest in terms of both theoretical and experimental researches [10−15]. Namely, the successful preparation of a polymer membrane composed of large quantities of CNTs arranged

in parallel makes it possible for macroscopic measurement of the trans-nanotube transportation [5,6,16]. By this method, it is proven that CNTs have a distinct advantage in fluid transport with four to five orders of magnitude faster than that predicted by conventional fluid-flow theory [11−13]. It is assumed that such a high flow velocity is attributable to the near-frictionless movement of liquid molecules along the walls of CNTs. Hydrophilic treatment can further enhance mass transfer rate of CNTs. For example, by functionalizing CNTs with carboxylic acid groups through plasma treatment, liquid flow through the cores of CNTs could be further accelerated by ~1,000-10,000 times faster than that predicted by the conventional no-slip hydrodynamic theory [11,17]. This finding indicates that surface modification of CNTs is a powerful method to improve their mass transport capability. However, for ion transportation through CNTs, the transport situation becomes much more complicated, although water is still the main transport medium [18−21]. It was found that, even after plasma treatments, ion diffusion through CNT was close to the bulk diffusion expectations and no obvious acceleration was detected [7]. Moreover, if there are charged groups near the CNT entrance, the transport of ions would be further hindered and even rejected due to the Donnan-type ion rejection mechanism [16].

Functionalization of CNTs with phospholipids is of significance for biomedical applications [22,23]. Modification of the CNT surface with PEGylated phospholipid molecules has been widely used to improve the aqueous stability and biocompatibility of CNTs [24−26]. It is assumed by some models that phospholipids would attach to the exterior walls of CNTs and even assemble into a helical structure [27−29]. However, to the best of our knowledge, few experimental studies have been reported on the assembly of phospholipids within the inner cores of CNTs, and particularly its impact on the ion transportation through CNTs, which is mostly

caused by difficulties in controllable filling of lipids into the CNT cavity and limitations in characterization methods [30−34].

In this work, based on the millimeter-sized CNT membrane comprising well aligned multi-wall carbon nanotubes (i.e., MWNT-membrane, with an inner size of ~10 nm), an inter-diffusion method was employed to incorporate phospholipid molecules into the CNTs under mild conditions. Another type of CNT membrane composed of Anodic Aluminium Oxide-based carbon tubes (i.e., AAO-CT-membrane, with an inner diameter of ~70 nm) was used as a reference. We found that lipids could stay inside the tubes or stack at their tips, depending on lipid types and surface properties of the inner walls of the tubes. Ionic transport tests showed the manner of lipid decoration on CNTs significantly influenced the behavior of ion transport through the tubes. Incorporation of lipids in the tube interior enhances ion transport rate by a factor of more than five, whereas CNT tip-exclusive lipid decoration would lead to an improvement during the initial ion transport stage only. These results provide a practical guide for designing advanced biomimetic nanoscale channels with controllable and high efficiency ion transportation.

2. Experimental Section

2.1 Materials

1,2-Dioleoyl-sn-glycero-3-phosphocholine (DOPC), 1,2-dipalmitoylsn-glycero-3-phosphocholine (DPPC), 1-palmitoyl-2-(9,10-dibromo)stearoyl-sn-glycero-3-phosphocholine (Br-PC), 1,2-di-(10Z,12Z-tricosadiynoyl)-sn-glycero-3-phosphocholine (Diyne-PC), and 1,2-dipalmitoyl-sn-glycero-3-phosphoethanolamine-N-(lissaminerhodamine B sulfonyl) (Rh-PE), were purchased from Avanti Polar Lipids and used as received (**Fig. 1**a). All other chemicals

(AR) were purchased from Sinopharm Chemical Reagent Co., Ltd. and used without further purification.

2.2 Preparation of MWNT- and AAO-CT-membrane

The MWNT-membrane was fabricated based on the preparation of a vertically-aligned MWNT-array as detailed in our previous reports [35,36]. Briefly, a 1−10 mm thick MWNT-array was first grown via the classical chemical vapor deposition (CVD) method on a Si wafer substrate. After sealing the tubes' tips with polypropylene, ethoxyline was employed to fill the spaces within the nanotube array, and this was followed by solidification. The bulk material was then sliced (parallel to the substrate) using a microtome (RMC, Boeckeler Instruments, Inc.) into freestanding membranes with a thickness of 10±1 μm. Oxygen plasma etching was then applied with a PDC-32G plasma cleaner (Harrick Plasma Inc.) to remove the organic residues around the tips of the CNTs (18 W for 20 min, O_2, 500 mtorr). The AAO-CT-membrane was fabricated by depositing a layer of amorphous carbon onto the porous AAO structure by the template method. After eliminating the carbon on both surfaces of the film, an aligned carbon tube membrane with penetrating pores was obtained [37].

2.3 Diffusion and ion transport test

Diffusion-unit set-up. The home-made diffusion unit was setup as demonstrated in Fig. 1b. The unit was comprised of two cells, A and B (both in resin, each with a pore 4 mm in diameter), and two spacers, E and F (in silicone, also had a 4 mm size pore in the middle). The solution in the two cells could communicate through the pores and the membrane sandwiched between the spacers. Each time for solution (or membrane) replacement, solutions in the two cells were

poured out simultaneously, and the unit was disassembled, washed completely and dried under N_2 flow for its next use.

Ion transport test. The tests were performed based on the diffusion procedure. The membrane was first installed within the diffusion unit. After that, 7 mL KCl solution (0.1 M and 0.5 mM) were filled into the feed and the permeate cells A and B, respectively. Thus, the total mass of KCl in the feed solution was more than two orders of magnitude greater than that in the permeate, effectively eliminating depletion effects. Such a concentration gradient led to the ionic transport across the membrane from A to B. The changes in electrical conductivity of the permeate (cell B) were monitored simultaneously during incubation by a water analyzer (Ultrameter II, Myron L Company).

Lipid decoration. Lipid decoration for the membrane was realized by a similar inter-diffusion method. A homogeneous lipid solution (0.2 mg mL^{-1}) was used as a mother solution. Briefly, a 700 μL lipid solution (2.0 mg mL^{-1}, containing 0.5 mol% Rh-PE for fluorescent labeling) was transferred into an ampoule (wrapped with tin foil paper), dried under an N_2 flow and kept in a vacuum overnight. The membrane was then rehydrated with 7 mL distilled water and sonicated for a complete dispersion of lipids. During lipid decoration, a naked carbon membrane was first installed within the diffusion unit. 7 mL lipid mother solution and distilled water were added into cells A and B, respectively. After incubation at room temperature for 48 h, a fluorescent signal of lipids can be detected from cell B, which indicates that the lipids have successfully permeated through the membrane. The membrane was then gently removed, washed with water and dried under N_2 flow for further experiments.

Experiment steps. For each carbon membrane, the experiment was carried out as follows. First, the naked membrane was set up for a KCl diffusion test in order to obtain baseline ion diffusion data. Second, the membrane wad decorated with lipids, followed by other characterizations including TEM and confocal imaging. Third, the carbon membrane was reassembled and step 1 was repeated so that the ionic diffusion rate of the membrane with incorporated lipids could be measured. Fourth, the KCl solution was renewed, and the membrane was washed and dried, then the ionic diffusion test was repeated, as described in the main text. Specifically, for lipid Diyne-PC, after step 3, the carbon membrane was removed, dried and placed on a glass slide under UV exposure for 30 min (285 nm wavelength) for lipid polymerization. Finally, the membrane was reassembled for the following ionic diffusion test.

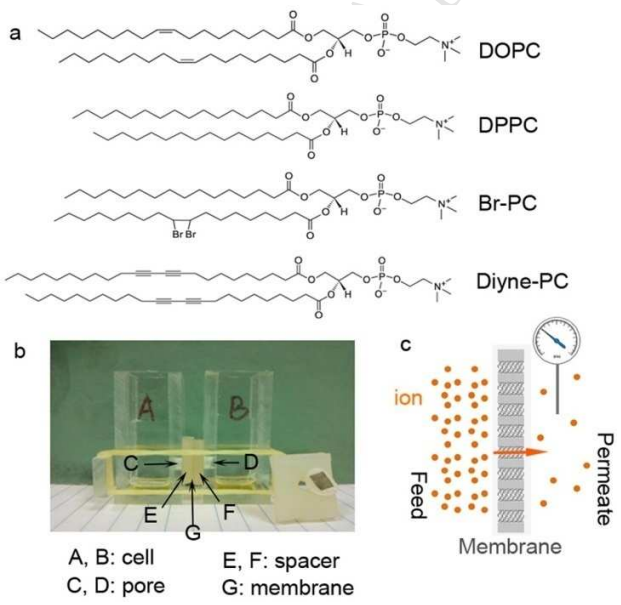

Fig. 1 Chemical structures of lipids and images demonstrating the diffusion unit and process. (a) Molecular structure of lipids DOPC, DPPC, Br-PC and Diyne-PC. (b) Digital photo of the diffusion unit, including cells (A, B) with pores on one side (C, D), spacers (E, F) with pores, and the sandwiched membrane (G; cannot be seen here). Another spacer (and membrane) was

placed aside for reference. (c) Schematic showing the transport of ions through CNTs within a membrane from the feed side to the permeate side.

2.4 Characterizations

The morphology of the carbon membranes was characterized with SEM (Hitachi S-4700, Hitachi). The structure of the lipids within the membrane was further characterized with TEM (FEI Tecnai G-20) at 200 kV and small angle X-ray scattering (SAXS) at Shanghai Synchrotron Radiation Facility (SSRF).

Optical observation was performed on an inverted confocal laser scanning microscope (LSM 710, Zeiss) equipped with a 100× oil objective. Rhodamine-conjugated phospholipids were excited by a He−Ne laser (EX 543 nm), and the fluorescence was observed through filter set 20 (EM BP 575−640 nm). In the meantime, the transmission channel illuminated with a halogen lamp was acquired. All experiments were carried out at room temperature.

3. Result and discussion

3.1 Characterization

Fig. 2 shows schematic and SEM images of the as-fabricated MWNT- and AAO-CT-membranes. For a MWNT-membrane with a thickness of 10±1 μm, the nanotubes, which are normal-oriented and parallel-aligned in the membrane, are clearly distinguishable from the cross-sectional image under SEM (Fig. 2b, c). On the other hand, for the AAO-CT-membrane, the carbon tubes with similar orientation and alignment have a much larger pore diameter of ~70 nm and a length of 43±4 μm. It is worth noting that the nanopores of CNTs are the only paths for mass transportation due to the impermeable polymer matrix (or AAO template). Thus, the

160 macroscopic transport measurements of ions through membrane were performed to determine
161 the transport through the inner cores of both types of CNTs [35].

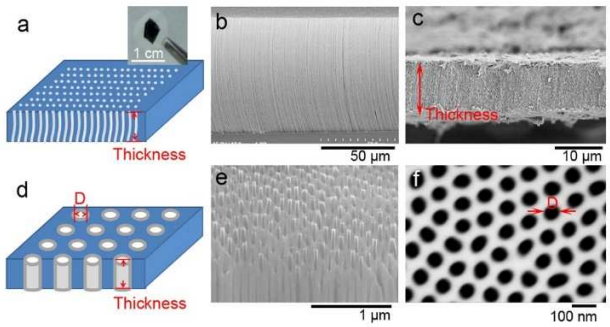

162

163 Fig. 2 Schematic and SEM images of the MWNT- (a-c) and AAO-CT- (d-f) membranes. (a)
164 Schematic, (a-inset) digital and (c) cross-sectional SEM images of a MWNT-membrane. (b)
165 presents the aligned MWNT array grown vertically on a substrate. (d) Schematic, (e) cross-
166 sectional and (f) top-view SEM images of an AAO-based amorphous CT-membrane.

167

168 The membrane was then sandwiched within the diffusion unit for lipid decoration and the
169 subsequent ion diffusion test. **Fig. 3** shows confocal fluorescence images of the MWNT- and
170 AAO-CT-membranes right after DOPC decoration. The membrane surfaces and location of the
171 fluorescent lipids can be distinguished from the transmission and red fluorescence channels,
172 respectively. Moreover, based on the three dimensional (3D) scanning, it was observed that for
173 the MWNT-membrane, the lipids were located within the interior of the CNTs (Fig. 3b, i).
174 However, for the AAO-CT-membrane, the lipids were uniformly distributed on the two ends of
175 the CNTs, with an inter-layer distance similar to the thickness of the initial AAO-CT-membrane
176 (Fig. 3d). Z-stack images of both membranes are shown for reference in Fig. S1 in the supporting
177 information. Here, DOPC is replaced with various other types of lipids, including DPPC (in gel

phase at room temperature), Diyne-PC (a kind of diacetylene phospholipid) and Br-PC (labeled with two Br atoms in each molecule). All the above-mentioned lipids share similar assembly states of CNTs with DOPC.

To obtain more details of the assembly method of lipids within CNTs, the scaffold (polymeric or AAO) membranes were digested and the CNTs (with loaded lipids) were redispersed and loaded on a lacey support membrane for TEM imaging. To have a good contrast under TEM, Br-PC and Diyne-PC were used here instead of DOPC or DPPC. **Fig. 3**e-g show TEM images of the MWNTs (with an inner core diameter of ~10 nm) without and with lipid decoration, from which the multilayer structure of the tube walls can be obviously distinguished (Arrow 1). It should be noted that for the native MWNTs, the cavity region is much dimmer in comparison with the wall region. However, for the lipid-decorated tubes, the cavity region is even darker in contrast with the walls (Arrow 3). This is reasonable considering that, compared with C, the P (and/or Br) atoms from the lipids contribute a much stronger influence on the electron beam during TEM imaging. This result further confirms the existence of lipids within the MWNTs (although a gap might appear somewhere between the wall and the encapsulated lipid molecules as indicated with Arrow 2) [37]. Furthermore, the dark region located continuously within the cavity, indicating an uninterrupted distribution of lipids along the tube. In contrast, similar morphologies were obtained for the AAO-CT membranes without and with lipid decoration. The inner core region is much dimmer than the wall region, indicating that hardly any lipid remains inside the amorphous carbon tubes (Fig. 2h). Synchrotron X-ray scattering was also carried out to characterize the lipid structure within both membranes. However, only signal of an ordered structure with a period of ~155 nm (Fig. S2), probably referring to the parallel-distributed amorphous carbon tubes (i.e. porous aluminum template), was acquired from the AAO-CT-

membrane. No signal of ordered lipid structures (such as lamellar or hexagonal assembly) was acquired from either membrane (Supporting Information).

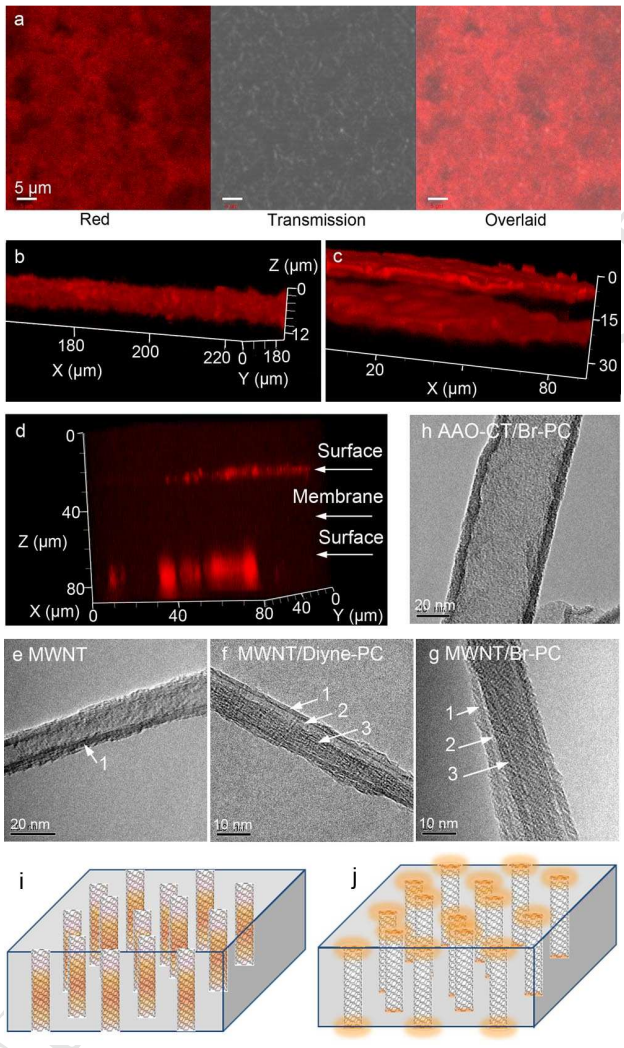

Fig. 3 Confocal fluorescence microscopy, TEM and schematic images of the MWNT/lipid and AAO-CT/lipid membranes. (a) Confocal 2D (in red fluorescence, transmission and overlaid channels) and (b-d) 3D images of the MWNT/DOPC (a, b) or AAO-CT/DOPC (d) composite membrane. (c) Redistribution of lipids within the MWNT/DOPC composite membrane after approximately five cycles of the ionic diffusion test. Red fluorescence comes from the Rh-labeled lipid. (e-h) TEM images of MWNT, MWNT/Diyne-PC, MWNT/Br-PC and AAO-

CT/Br-PC samples. Arrows 1-3 refer to the graphite layer, the gap and the encapsulated lipid molecules, respectively. (i, j) Schematics representing the relative locations of fluorescent lipids and CNTs within a MWNT/DOPC membrane, corresponding to (b) and (c), respectively.

3.2 Influence from lipid decoration on ion transport rate through tubes

Ion transport rates through tubes both with and without lipid decoration were measured based on the concentration-driven diffusion of KCl across the membranes. The membranes were fixed between a feed cell and a permeate cell within the diffusion unit, and the concentration gradient between the two cells led to ion diffusion through tubes (Fig. 1b, c). Based on the time-dependent increase in conductivity of the solution in the permeate cell, the ion transport rate across the tubes was obtained. Furthermore, for the native MWNT-membrane, the conductivity values were used to calculate the permeable pore area (cm^2) and density ($\#/cm^2$) which can satisfactorily characterize the permeability of the membrane (Supporting Information, Section S2). On the other hand, for the tubes with lipid decoration, the influence from lipid functionalization was described by comparing the ion transport rate of each membrane before and after lipid decoration, and consequently an average from more than three independent samples was calculated. This is suspected to be more direct and accurate concerning the deviation among various membrane samples.

Fig. 4 shows the time-lapse distribution of conductivity of the solution in the permeate cell, corresponding to the ion transport rate through a membrane. For the native MWNT-membrane (Fig. 4a, in black), the changes in conductivity are characterized with two typical stages: in Stage I, the value increases quickly, referring to a fast transport of ions through tubes; then, in Stage II, the value increases gradually with a linear dependence on time, indicating a dynamically-

balanced transfer of ions in the tubes. Moreover, based on the steady state flux in Stage II, the permeable pore density of our MWNT-membranes was calculated to be $2.2\pm0.2\times10^{8}$ cm^{-2}, which indicates a good permeability of the membrane (i.e., tubes in the membrane).

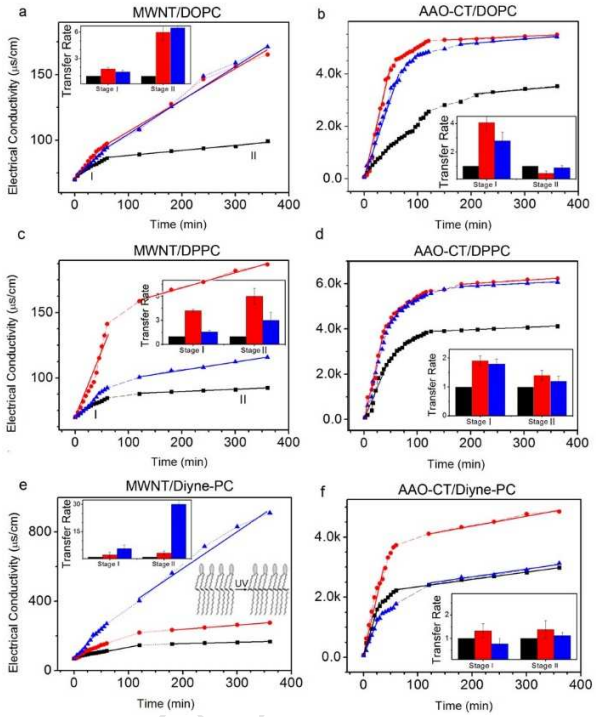

Fig. 4 Electrical conductivity changes with time for the diffusion solution during KCl transfer process through typical MWNT/lipid (a, c, e) or AAO-CT/lipid (b, d, f) membranes. Insets, corresponding ion transport rate calculated from the electrical conductivity distribution (normalized by the value of the naked carbon membrane and averaged from 3 independent samples). The black curve/histogram refers to the naked carbon membrane while the red (or blue) one refers to that in the first (or repeated) ionic diffusion test; in (e, f), the red and blue curves refer to the membrane before and after UV polymerization of Diyne-PC, respectively. Right-inset in (e), schematic diagram demonstrating the polymerization of Diyne-PC lipids under UV exposure.

After DOPC decoration, obvious changes appear (Fig. 4a, in red). The evolution of conductivity still shows a typical two-stage process, but the corresponding values experience a significant increase. By fitting the conductivity profile, ion transport rates through tubes were obtained. Before lipid decoration, the ion transport rates in stages I (concerning the almost linear period before 60 min) and II are 3.13×10^{-10} and 4.68×10^{-11} moles s^{-1}, respectively. After DOPC decoration (in red), factors of ~2 (for Stage I, analyzed from more than three independent samples) and ~5 (for Stage II) times increases occur (Fig. 4a, inset). Such improvements clearly suggest that the assembly of lipids in the tube's interior is able to enhance ion transport through CNTs.

Moreover, ion transport through tubes is significantly affected by the location and/or assembly of lipids within tubes. Compared with the MWNT-membrane, the ion transport rate in the AAO-CT-membrane only increases slightly during Stage I (from ~2.75×10^{-8} to ~9.78×10^{-8} moles s^{-1}, referring to the typical membrane shown in Fig. 4b), while in Stage II, the value recovers to its pre-lipid modification state (of around 2.2×10^{-9} moles s^{-1}). Note that in this case lipids mainly accumulate at the tips of the tubes while small molecules remain inside of the tubes.

The type of lipid used in lipid decoration also has an impact on the enhancement effect on ion transport through tubes. For the MWNT/DOPC composite membrane, it was found that in repeated ion-transport tests (after drying and rehydration of the membrane as stated in the experimental section), the conductivity profile (Fig. 4a, in blue) almost overlaid with the initial one (in red). This indicates that the enhancement effect on ion transport (i.e. the stability of lipid decoration within tubes) is relatively stable. However, when we replaced DOPC with DPPC which exists in gel phase at room temperature (Fig. 4c, black and red), it was found that the

lipid-induced enhancement on ion transport occurred only in the first measurement (with an enhancement rate being similar to that of DOPC); whereas in the following repeated cycles, the ion transport rate recovers to the level of a case without lipid decoration (except for an enhancement in Stage Ⅰ). In fact, even for DOPC decoration, after a repetition of 3-5 cycles, the escape of DOPC molecules from the interior to the tips of the tubes (Fig. 3c), and the corresponding recovery in ion transport rate, were observed. On the other hand, for the AAO-CT-membrane, no obvious difference was observed when DOPC was replaced with DPPC, indicating the stable accumulation of lipids at the tips of this type of tubes (Fig. 4d).

The stability of lipid decoration, especially inside the tubes, is crucial for practical applications. To conquer this, another type of diacetylene lipid, Diyne-PC, was employed. It is known that under UV radiation, the adjacent tails of Diyne-PC lipids tend to polymerize with covalent bonds, leading to the formation of a continuous π bond within the layer [38]. This significantly improves the stability of the assembled lipid structure (Fig. 4e right-inset). By the same concentration-driven method, Diyne-PC was incorporated into the MWNT-membrane, which showed a similar distribution as that of DOPC inside the CNTs (Fig. S3a,b). UV irradiation was then performed to polymerize the lipids. Fluorescence spectra of model membranes before and after lipid polymerization are shown in Fig. S3c-e to confirm the successful polymerization of lipids within membrane.

Fig. 4e shows the conductivity profiles for the condition of model MWNT-membrane, with and without Diyne-PC incorporation, both before and after UV-polymerization. Before UV irradiation, the influence of Diyne-PC decoration on steady ion transport rate was similar to (although lower than) that of DOPC, with a 3-4 times enhancement (Fig. 4e in red); however, in a sharp striking contrast, after polymerization, the steady ion transport rate was increased up to

20 times larger than that of the native membrane (Fig. 4e in blue). Furthermore, repeated tests showed a good stability of such a promoted transport rate even after more than five cycles' test. However, for the AAO-CT/Diyne-PC composite membrane (Fig. S3b), UV-polymerization had little effect on the steady ionic transport (Fig. 4f).

3.3 Discussion

By an inter-diffusion method, lipids were successfully incorporated into CNTs. According to our results, lipids can self-assemble inside or outside the tubes, probably depending on the surface properties of the inner-walls of the tubes and the phase state of lipids. For MWNTs, the strong affinity between the alkyl tails of lipid molecules and the hydrophobic aromatic plane of tubes facilitates the localization of lipids within the interior of the tubes (Supporting Information, Section S3). However, for AAO-CTs, the hydrophilic surface of the amorphous carbon layer makes it difficult for lipids to stay inside the tubes, although it is much easier for an assembled lipid layer to attach to a less curved surface (i.e. AAO-CTs with a larger size) in comparison with a highly curved one (i.e. MWNT with a smaller size; Supporting Information, Section S4). Furthermore, in comparison with gel-phase DPPC, the flexible tails of liquid-phase DOPC promotes the assembly and localization of lipids on the highly-curved inner surface of CNTs as a result of a much lowered energy cost for layer bending (Supporting Information, Section S4).

It is clearly demonstrated that the assembly of lipids inside the MWNTs significantly facilitates the ion transport through the tubes, on the basis of confocal, TEM and ion transport tests. Moreover, polymerization of Diyne-PC inside the tubes further enhances the steady ion transport compared with that of DOPC/DPPC; this is probably due to the more uniform and stable distribution of lipid molecules caused by inter-molecule binding between adjacent Diyne-PCs. In addition, accumulation of lipids at the tips of the CNTs could also boost the ion transport

rate at the initial stage, although without much influence on the steady ion transport process. These results all promise the regulation of ion transportation behaviors through CNTs for practical applications.

The influence of lipid decoration on ion transport is suspected to be associated with the complicate ion-lipid interactions, which could create a preferred distribution of ions near the zwitterionic lipid headgroups [39−41]. Electroneutral or negatively charged molecules were also used instead of the zwitterionic lipids for MWNT decoration, which, however, reduced the ion transport rate (Fig. S4). In this regard, the accumulated lipids at tube-tips would increase the local ionic concentration at the tube entrance, and consequently enhance the ion transport under the effect of flow during the initial period (i.e. Stage I). In contrast, the incorporation and continuous localization of lipids along the tubes might provide successional binding sites for ions with lipid headgroups, which could work as a highway for the ion transport throughout the whole tube, and thus significantly increase the steady ion transport rate (although the pore size might decrease due to lipid incorporation). The remarkable increase in ion transport due to the polymerized Diyne-PC decoration further confirms this speculation.

4. Conclusion

In this study, we prepared two types of vertically-aligned CNT membranes composed of MWNTs or AAO-based amorphous CNTs, and investigated the influence of lipid decoration on the ion transport properties through the inner core of the nanotubes via macroscopic transport measurements. Concentration-driven diffusion was employed for the incorporation of lipids within the tubes. Confocal imaging and TEM observation indicated the continuous distribution of lipids inside the MWNTs, probably due to the hydrophobic interaction between the alkyl tails

of lipids and the aromatic wall plane of MWNT. In contrast, for the AAO-CT-membrane, lipids tended to accumulate at the two sides of the membrane, likely at the tips of the carbon tubes. Ion transport tests demonstrated an enhancement in the steady ion transport rate through MWNTs due to lipid incorporation, by approximately 5 times for DOPC or DPPC, 3-4 times for Diyne-PC, and up to 20 times for Diyne-PC after polymerization. Furthermore, the accumulation of lipids at the tips of the carbon tubes (both MWNTs and AAO-CTs) accelerated the ion transport during the initial stage, but hardly influenced the steady transport rate of ions. The increase in local ionic concentration due to the binding of ions to zwitterionic headgroups of the decorated lipids is supposed to be one of the key factors for the enhanced ion transport rate. Our results provide promising possibilities for selective and high-efficiency transport of CNTs for separation and sensing applications [16], after further functionalization of lipids.

Acknowledgments

This work was financially supported by the National Science Foundation of China (Nos. 91427302, 21422404, 21374074, U1532108 and 11474155). The authors sincerely thank Prof. Guowen Meng (Institute of Solid State Physics, Chinese Academy of Sciences) for providing the AAO-based CT-membrane. The authors also thank the Small Angle X-ray Scattering Station (BL16B) and X-ray Diffraction Station (BL14B) at Shanghai Synchrotron Radiation Facility (SSRF) for sample characterizations.

Appendix A. Supplementary data

Confocal z-stack images of the MWNT/DOPC and AAO-CT/DOPC composite membranes; synchrotron SAXS pattern of the AAO-CT/DOPC membrane; confocal 3D images and PL profiles of the MWNT/Diyne-PC and AAO-CT/Diyne-PC membranes; ion transport through

MWNT membranes after PS-PAA or calcein decoration; estimation of the permeable pore area and density from KCl diffusion measurements; interaction energy analysis between components of a lipid-decorated MWNT system; energetic analysis of DOPC and DPPC assemblies in MWNTs. These materials can be found, in the online version, at …

REFERENCES

[1] Hong GS, Diao S, Antaris AL, Dai HJ. Carbon nanomaterials for biological imaging and nanomedicinal therapy. Chem Rev 2015; 115(19): 10816–10906.

[2] Mehra NK, Jain NK. Multifunctional hybrid–carbon nanotubes: new horizon in drug delivery and targeting. Journal of Drug Targeting. J Drug Target 2016; 24(4): 294–308.

[3] Sajid MI, Jamshaid U, Jamshaid T, Zafar N, Fessi H, Elaissari A. Carbon nanotubes from synthesis to in vivo biomedical applications. Int J Pharm 2016; 501(1–2): 278–299.

[4] Mehra NK, Jain AK, Lodhi N, Raj R, Dubey V, Mishra D, et al. Challenges in the use of carbon nanotubes for biomedical applications. Crit Rev Ther Drug Carrier Syst 2008; 25(2): 169–206.

[5] Majumder M, Stinchcomb A, Hinds BJ. Towards mimicking natural protein channels with aligned carbon nanotube membranes for active drug delivery. Life Sci 2010; 86(15–16): 563–568.

[6] Hinds B. Dramatic transport properties of carbon nanotube membranes for a robust protein channel mimetic platform. Curr Opin Solid St M 2012; 16(1): 1–9.

[7] Majumder M, Chopra N, Hinds BJ. Mass transport through carbon nanotube membranes in three different regimes: ionic diffusion and gas and liquid flow. ACS Nano 2011; 5: 3867–3877.

[8] He Z, Zhou J, Lu X, Corry B. Bioinspired graphene nanopores with voltage-tunable ion selectivity for Na^+ and K^+. ACS Nano 2013; 7(11): 10148–10157.

[9] He Z, Corry B, Lu X, Zhou J. A mechanical nanogate based on a carbon nanotube for reversible control of ion conduction. Nanoscale 2014; 6: 3686–3694.

[10] Whitby M, Quirke N. Fluid flow in carbon nanotubes and nanopipes. Nat Nanotechnol 2007; 2: 87–94.

[11] Majumder M, Chopra N, Andrews R, Hinds BJ. Enhanced flow in carbon nanotubes. Nature 2005; 438: 44.

[12] Hummer G, Rasaiah JC, Noworyta JP. Water conduction through the hydrophobic channel of a carbon nanotube. Nature 2001; 414: 188–190.

[13] Rivera JL, Starr FW. Rapid transport of water via a carbon nanotube syringe. J Phys Chem C 2010; 114: 3737–3742.

[14] Cohen-Tanugi D, Grossman JC. Water Desalination across Nanoporous Graphene. Nano Lett 2012; 12: 3602–3608.

[15] Pham TA, Golam Mortuza SM, Wood BC, Lau EY, Ogitsu T, Buchsbaum SF, et al. Salt solutions in carbon nanotubes: the role of cation− π interactions. J Phys Chem C 2016; 120(13): 7332–7338.

[16] Hinds BJ, Chopra N, Rantell T, Andrews R, Gavalas V, Bachas LG. Aligned multiwalled carbon nanotube membranes. Science 2004; 303(5654): 62–65.

399 [17] Moskowitz I, Snyder MA, Mittal J. Water transport through functionalized nanotubes with
400 tunable hydrophobicity. J Chem Phys 2014; 141(18): 18C532.

401 [18] Yu M, Funke HH, Falconer JL, Noble RD. Gated ion transport through dense carbon
402 nanotube membranes. J Am Chem Soc 2010; 132: 8285–8290.

403 [19] Pan Y, Wu Q, Weng Y, Zhang X, Yang Z, Meng J, et al. Declined ionic flux through the
404 nano-pores of vertically aligned carbon nanotubes filled with PNIPAm hydrogel. J Mater Chem
405 A 2015; 3: 11111–11116.

406 [20] Zhu Y, Guo X, Shao Q, Wei M, Wu X, Lu L, et al. Molecular simulation study of the
407 effect of inner wall modified groups on ionic hydration confined in carbon nanotube. Fluid Phase
408 Equilibria 2010; 297: 215–220.

409 [21] He Z, Zhou J, Lu X, Corry B. Ice-like water structure in carbon nanotube (8,8) induces
410 cationic hydration enhancement. J Phys Chem C 2013; 117: 11412–11420.

411 [22] Kim SW, Kim T, Kim YS, Choi HS, Lim HJ, Yang SJ, et al. Surface modifications for the
412 effective dispersion of carbon nanotubes in solvents and polymers. Carbon 2012; 50(1): 3–33.

413 [23] Wu Y, Hudson JS, Lu Q, Moore JM, Mount AS, Rao AM, et al. Coating single-walled
414 carbon nanotubes with phospholipids. J Phys Chem B 2006; 110: 2475–2478.

415 [24] Diao S, Blackburn JL, Hong GS, Antaris AL, Chang JL, Wu JZ, et al. Fluorescence
416 imaging in vivo at wavelengths beyond 1500 nm. Angew Chem Int Edit 2015; 54(49): 14758–
417 14762.

418 [25] Liang C, Diao S, Wang C, Gong H, Liu T, Hong G, et al. Tumor metastasis inhibition by
419 imaging-guided photothermal therapy with single-walled carbon nanotubes. Adv Mater 2014;
420 26(32): 5646–5652.

421 [26] Hong G, Diao S, Chang J, Antaris AL, Chen C, Zhang B, et al. Through-skull
422 fluorescence imaging of the brain in a new near-infrared window. Nat Photonics 2014; 8(9):
423 723–730.

424 [27] Islam MF, Rojas E, Bergey DM, Johnson AT, Yodh AG. High weight fraction surfactant
425 solubilization of single-wall carbon nanotubes in water. Nano Lett 2003; 3(2): 269–273.

426 [28] Giulianini M, Waclawik ER, Bell JM, De Crescenzi M, Castrucci P, Scarselli M, et al.
427 Regioregular poly(3-hexyl-thiophene) helical self-organization on carbon nanotubes. Appl Phys
428 Lett 2009; 95(1): 013304.

429 [29] Maatta J, Vierros S, Sammalkorpi M. Controlling carbon-nanotube-phospholipid
430 solubility by curvature-dependent self-assembly. J Phys Chem B 2015; 119(10): 4020–4032.

431 [30] Arai N, Yasuoka K, Zeng XC. Phase diagrams of confined solutions of
432 dimyristoylphosphatidylcholine (DMPC) lipid and cholesterol in nanotubes. Microfluid
433 Nanofluid 2012; 14(6): 995–1010.

434 [31] Arai N, Yasuoka K, Zeng XC. Self-assembly of surfactants and polymorphic transition in
435 nanotubes. J Am Chem Soc 2008; 130: 7916–7920.

436 [32] Khlobystov AN, Britz DA, Briggs GAD. Molecules in carbon nanotubes. Accounts Chem
437 Res 2005; 38(12): 901–909.

438 [33] Gautam UK, Costa PMFJ, Bando Y, Fang XS, Li L, Imura M, et al. Recent developments
439 in inorganically filled carbon nanotubes: successes and challenges. Sc Technol Adv Mater 2010;
440 11(5): 054501.

441 [34] Muter D, Shin T, Deme B, Fratzl P, Paris O, Findenegg GH. Surfactant self-assembly in
442 cylindrical silica nanopores. J Phys Chem Lett 2010; 1(9): 1442–1446.

443 [35] Liao G, Pan Y, Wu Q, Li S, Weng Y, Zhang X, et al. A novel method to encapsulate a Au
444 nanorod array in 15 nm radius multiwalled carbon nanotubes. Nanoscale 2014; 6: 14872–14876.

445 [36] Liu Z, Liao G, Li S, Pan Y, Wang X, Weng Y, et al. Efficient encapsulation of conducting
446 polyaniline chains inside carbon nanotubes: a new strategy to prepare endohedral CNT materials.
447 J Mater Chem A 2013; 1(42): 13321–13327.

448 [37] Jani AMM, Losic D, Voelcker NH. Nanoporous anodic aluminium oxide: advances in
449 surface engineering and emerging applications. Prog Mater Sci 2013; 58(5): 636–704.

450 [38] Yuan B, Hu S, Lu N, Xu F, Zhou K, Ma Y, et al. Electrical bistability in self-assembled
451 hybrid multilayers of phospholipid and nanoparticles. Nanotechnology 2011; 22(31): 315303.

452 [39] Vacha R, Berkowitz ML, Jungwirth P. Molecular model of a cell plasma membrane with
453 an asymmetric multicomponent composition: water permeation and ion effects. Biophys J 2009;
454 96(11): 4493–4501.

455 [40] Klasczyk B, Knecht V. Validating affinities for ion-lipid association from simulation
456 against experiment. J Phys Chem A 2011; 115(38): 10587–10595.

457 [41] Seelig J, MacDonald PM, Scherer PG. Phospholipid head groups as sensors of electric
458 charge in membranes. Biochemistry 1987; 26(24): 7535–7541.